Interaction of human Crx and Nrl in live cells measured using fluorescence resonance energy transfer (FRET)

Xinming Zhuo[1] and Barry E. Knox

Affiliations:
Departments of Ophthalmology & Visual Sciences and Biochemistry & Molecular Biology, Center for Vision Research, SUNY Upstate Medical University, Syracuse, NY 13210, USA
[1]Current address: CLIA Laboratory, The Jackson Laboratory for Genomic Medicine, University of Connecticut Health Center, 10 Discovery Dr., Farmington, CT 06032
xmzhuo@gmail.com

Key words: cone-rod homeobox (Crx), neural retina leucine zipper (Nrl), fluorescence resonance energy transfer (FRET), flow cytometry, confocal microscopy, transcription factors, DNA binding protein, fluorescent proteins, gene expression, retina, rod photoreceptor

Please send correspondence to:
Barry E. Knox, Ph.D.
Department of Ophthalmology & Visual Sciences
Neuroscience Research Building, Room 3613
SUNY Upstate Medical University
505 Irving Avenue
Syracuse, NY, USA
Phone: 315-464-8719
knoxb@upstate.edu

Abstract

Crx and Nrl are retina-specific transcription factors that control rod photoreceptor differentiation and synergistically activate rod phototransduction gene expression. Previous experiments showed they interact *in vitro* and in yeast two-hybrid assays. Here, we examined Crx-Nrl interaction in live HEK293T cells using two fluorescence resonance energy transfer (FRET) approaches: confocal microscopy and flow cytometry (FC-FRET). FC-FRET can provide measurements from many cells having wide donor-acceptor expression ranges. FRET efficiencies were calibrated with a series of donor (eGFP)-acceptor (mCherry) fusion proteins separated with linkers between 6-45 amino acids. Crx and Nrl were fused at either terminus with eGFP or mCherry to create fluorescent proteins, and all combinations were tested in transiently transfected cells. FRET signals between Crx or Nrl homo-pairs were highest with both fluorophores fused to the DNA binding domains (DBD), lower with both fused to the activation domains (AD), and not significant when fused on opposite termini. Nrl had stronger FRET signals than Crx. A significant FRET signal between Crx and Nrl hetero-pairs was detected when donor was fused to the Crx DNA binding domain and the acceptor fused to the Nrl activation domain. FRET signals increased with Crx or Nrl expression levels at a rate much higher than expected for collisional FRET alone. Together, our results show the formation of Crx-Nrl complexes *in vivo* that are close enough for FRET.

Introduction

Vertebrate photoreceptors express a large array of genes (1) specifically related to phototransduction (2) and their unique cellular structures (3, 4), such as the outer segment (5, 6). Crx (7-9), an Otx-like protein that is a member of the *paired* homeodomain family, and Nrl (10, 11), a basic leucine zipper (bZIP) protein that is a member of the large Maf family, are key retinal transcription factors essential for photoreceptor function. Together, they regulate rod photoreceptor differentiation and gene expression (12, 13), are involved in the *in vitro* differentiation of stem cells into photoreceptors (14-17) and are implicated in human retinal diseases (18-22). Moreover, Crx and Nrl are expressed in medulloblastoma cells, where they activate photoreceptor genes and contribute to tumor maintenance (23). In addition to a direct role in causing retinal disease via alterations of their protein sequence, they also play an indirect role by regulating genes that cause inherited retinal degenerative diseases. For example, there are more than 90 genes linked to one or more of six commonly occurring retinal diseases (24). Many of these genes are directly regulated by Crx or Nrl (25) or have putative cis-regulatory DNA binding sites close to their transcription initiation sites (26). Crx and Nrl together regulate transcription initiation of numerous genes (26, 27) directly by binding to *cis*-regulatory elements in promoter regions (26-29), indirectly through chromatin modification (30-32), and by interacting with or regulating other transcription factors (10, 25).

A thorough understanding of Crx and Nrl structure and function is essential, not only for establishing the mechanistic basis of photoreceptor gene expression, but for developing new treatments for human disease. Genome-wide analysis has identified a consensus Crx (26, 33) and Nrl (34, 35) cis-regulatory sequences that cluster in or near

rod photoreceptor genes, suggesting that Crx and Nrl together regulate them (26, 33). The localization of Crx-Nrl sites in proximal promoter regions reinforces functional and biochemical experiments that demonstrate cooperative action by Crx and Nrl to increase transcription (7, 36-38). In transiently transfected cultured cell lines, Crx and Nrl can individually activate transcription from rhodopsin and other photoreceptor-specific promoters, but together they do so synergistically (7, 36, 37). Crx and Nrl can bind to each other *in vitro* in the absence of DNA and can interact *in vivo* as inferred from yeast two-hybrid studies (36). Although the Nrl bZIP domain and the Crx homeodomain have roles in Crx-Nrl interaction *in vitro*, interaction appears to involve other regions of both proteins as well (36). Little is known about the underlying structural interface(s) that mediate complex formation, the structural basis for their transcriptional activity, protein-DNA or protein-protein interactions. The importance in understanding the structure-function relationships that result in Crx-Nrl cooperative transcriptional activity is highlighted by the fact that mutations in Crx or Nrl that reduce synergistic transactivation in cell transfection assays are linked to human retinopathies (20).

In this report, we describe the *in vivo* characterization of the interactions between Crx and Nrl in cultured mammalian cells. We utilized transiently transfected HEK293 cells, in which Crx-Nrl synergistically activate phototransduction gene promoter in transient transfection approaches (7, 36, 37). To measure FRET in living cells (39), we used either an improved FC-FRET approach, described here, or confocal microscopy FRET, CM-FRET (40). CM-FRET offers subcellular spatial resolution and the potential to observe movements of FRET partners by photobleaching methods (reviewed in (41, 42)). However, data collection with CM-FRET can be limited by both the number of cells that

can be processed and biases in cell selection. Previously, flow cytometry has been used for analysing FRET in populations of cells (43-51), including the interaction of transcription factors (49, 52). We adapted one FC-FRET method (49) in order to measure sensitized emission derived from donor-acceptor pairs and calibrated it using mCherry-eGFP (mG) fusion proteins separated by different length linkers. Using a combination of microscopy and flow cytometry, we characterized the interactions in living cells of Crx and Nrl fused to mCherry or eGFP and show interactions between these two transcription factors that are close enough for FRET.

Results

Measurement of FRET by flow cytometry.

Transiently transfected HEK293T cells have served as a convenient and rapid model system for the characterization of retinal transcription factors *in vivo* (e.g. (37)). We adapted an FC-FRET approach to measure apparent FRET efficiencies (N_{FRET}) determined by sensitized emission. For these studies, eGFP served as the donor and mCherry as the acceptor. Since our goal was to examine FRET between transcription factors, all protein constructs had a nuclear localization signal added to the N-terminus to direct expression exclusively to the nucleus. For each FC-FRET experiment (Figure S1), four control groups of cells were transfected with the following expression constructs: mock (empty pcDNA3.1), mCherry alone, eGFP alone, and unlinked mCherry plus eGFP (mCh+eG). Previous approaches estimated FRET by counting the number of cells that cross a threshold level of corrected F^{DA} intensity (Figure S2). In order to quantify FRET

signals, we employed a well-established method (three cube, (53)) to determine N_{FRET} on a cell-by-cell basis. Subsequently, the population averages and partitions based upon donor-acceptor intensity levels were used. The four control groups were used to estimate expression levels (Figure S3) and background–bleed-through fluorescence (crosstalk) in the FRET channel (Figure S4). To calibrate actual FRET signals (Figures 1, S4, and S5), we used donor-acceptor fusion proteins (mG) which undergo intramolecular FRET when eGFP is excited. The fusion was accomplished through linkers (Supplemental Table 1) containing an α-helix-forming peptide, EAAAK (54) repeated 2 to 7 times, and flanked on each side by a proline residue to terminate the α-helical region. For both unlinked and mG constructs, fluorescence was observed uniformly in the nucleoplasm (Figure S6). There was an enrichment in the nucleolus compared to the nucleoplasm, with a mean ratio of ~2 for both donor and acceptor fluorescence (*data not shown*). This is consistent with the behaviour of NLS which mediate RNA binding and nucleolar localization of fluorescent proteins (55).

FC-FRET produces sufficient cell numbers to restrict analysis to those that optimize the FRET signal to noise ratio (*e.g.*, Figure 1). To control for fluorescent protein expression levels which ranged over three orders of magnitude ($<10^{-7}$ to ~2 $x10^{-4}$ M, Figure S4), low expressing cells (with donor/acceptor fluorescence <~3 x 10^3 FU, Figures S4, S5) were eliminated from analysis (Figure S5). Only cells with an expression ratio for mCherry:eGFP between 0.1 -10, the range over which the FRET efficiency is most stable (56), were included. A criterion F^{DA} level (fluorescence intensity in the acceptor channel when excited with the donor laser) was set so that no cells that expressed either mCherry or eGFP alone reached this F^{DA} intensity (Figure S5, similar to a previous report (43)).

Cells that meet the above criteria F^{DA} intensity were termed FRET-positive cells. With this optimization, ~80.0% mG fusion construct expressing cells and ~4-5% of mCh+eG expressing cells were classified as FRET-positive in typical experiments (Figures S4 and S5) and were used to calculate N_{FRET}. In a typical experiment, we observed a mean N_{FRET} for mG10 expressing cells, expected to have a high FRET efficiency, that ranged from 21-24% while mCh+eG cells, expected to exhibit background FRET efficiency, was less than 1.5% (Figures 1A and S5). This represents an order of magnitude range for comparison of N_{FRET} in transfected HEK293T cells.

In addition to the intrinsic FRET that depends on the close proximity of donor-acceptor fluorophores, stochastic or collisional FRET arises from transient interactions between donor and acceptor (57). Stochastic FRET is expected to linearly depend upon the concentration of freely diffusing donors and acceptors (57-59). To estimate the contribution of stochastic FRET to the signal measured by flow cytometry, we examined cells expressing mG fusion proteins with a wide range of acceptor and donor fluorescence levels (Figure S6). This is readily accomplished since the FRET signals are collected over the entire range of mG expression during flow cytometry (Figure S7). In cells expressing mCh+eG, N_{FRET} modestly increased as either acceptor (Figures 1B and S7A) or donor (Figure S7B) fluorescence levels increased. The dependence of N_{FRET} on acceptor concentration fit the stochastic FRET equation ((57-59), Figure S8), indicating that the mCh+eG samples gave an accurate measure of the stochastic FRET component. We also compared collisional FRET in cells expressing nuclear-localized mCh+eG with those expressing cytoplasmic mCh+eG and found the dependence on expression level was indistinguishable in the two cellular compartments (Figure S9), further supporting the

identification of the mCh+eG signal with stochastic FRET. To characterize intrinsic FRET in the following experiments, we compared a population measure of FRET encompassing a range of expression levels (N_{FRET}) and the FRET efficiency dependence on fluorophore concentration.

Measurement of distance by FC-FRET.

To quantify FRET efficiencies as a function of donor-acceptor distance, we analysed N_{FRET} from cells expressing mG fusion proteins with different linker lengths (Figure 1A, Figure S6). The linker design incorporated a rigid alpha helix (54) that has been studied by X-ray analysis and shown to influence FRET efficiency in a fusion protein between BFP and GFP *in vitro* (60-62). The two proline residues incorporated in the mG design should isolate the alpha helical segments proteins to reduce influences of relative orientation of the two fluorophores. Fusion proteins with linkers less than 15 amino acids all exhibited similar N_{FRET} either in single or when averaging multiple FC-FRET experiments (mG6-8, one way ANOVA: $\alpha=0.05$, $F=1.54$, $p=0.29$; mG10 and mG15, t-test: mG-8 vs. mG10, $p=0.227$; mG-8 vs. mG15, $p=0.116$). N_{FRET} was very sensitive to lengths longer than 15 amino acids, with a steady reduction as linkers lengthened in individual (Figure 1A, *left*) or combined (Figure 1A, *right*) FC-FRET experiments (one way ANOVA, Holm-Sidak, pairwise comparison, all pairs have $p<0.05$).

All mG fusion proteins exhibited an increase in FRET efficiency as acceptor (Figures 1B and S7A) or donor (Figure S7B) fluorescence intensities increased, but the vertical offsets and slopes varied. The mG series of fusion proteins had parallel curves that differed in the offset at all fluorescence levels (Figures 1B and S7). This offset

191 depended upon the linker length and represented the intrinsic FRET from the donor-
192 acceptor pairs. There was a gradual increase in the slope at higher expression levels
193 which was similar for all mG fusion proteins and was greater than that for mCh+eG. The
194 cause of the increasing slope at higher tethered mCh+eG concentrations compared to
195 untethered fluorophores is not clear; it may be due to multiple donor-acceptor interactions,
196 either from concentration dependent association of fluorophores or collisions between
197 tethered fluorophores. The effect of donor-acceptor expression level on FRET signals
198 highlights the importance of comparing donor-acceptor pairs in the same concentration
199 range to clearly distinguish the intrinsic and stochastic FRET signals in transfected cells
200 (57-59).

201 To estimate the dependence of FRET efficiency on distance, R, between donor
202 and acceptor, we fit N_{FRET} to the Förster equation (Figure 1C): $N_{FRET} = \frac{R_o^6}{R_o^6 + (k_1 R + k_2)^6}$
203 where R_o is Förster distance (5 nm for eGFP and 4.7 - 5.2 nm for mCherry (63-65)), k_1 an
204 orientation factor between the fluorescent proteins, and k_2 is the minimal distance
205 between two fluorophores determined by steric exclusion. The data was well fit to this
206 equation using the predicted lengths of the alpha helical linkers (60-62). These results
207 show that FC-FRET can quantitatively measure small differences in distance between
208 donors and acceptors in living cells.
209

210 **Comparison of flow cytometry and confocal microscopy FRET**

211 We compared confocal microscopy and flow cytometry FRET with transfected cells
212 expressing either mG10 or mCh+eG (Figure 2). Using sensitized emission CM-FRET
213 (Figure 2A, B), cells expressing mG10 had a mean N_{FRET} of 9.9% (SD = 2.7%, n=37)

while cells expressing mCh+eG had a mean N_{FRET} of 0.80% (SD = 1.09%, n=31). This is likely an underestimate of the actual FRET efficiency because sensitized emission methods are very sensitive to instrument settings and crosstalk between donor and acceptor channels. Using acceptor photobleaching CM-FRET (66) on fixed cells to eliminate diffusion into and out of the photobleached region (Figure 2C-E), cells expressing mG10 had a mean N_{FRET} of 26.8% (SD = 4.4%, n = 37) while cells expressing mCh+eG, had a mean N_{FRET} of 0.0% (SD = 2.2%, n= 31). For comparison, a typical FC-FRET experiment is shown (Figure 2G) where the mean N_{FRET} was 23.5% (SD=3.8%, n=6987), while for mCh+eG cells N_{FRET} was 0.4% (SD = 1.4%, n = 5267).

There is a wide range of expression levels in transiently transfected cells (Figures S3 and S5), but the large number of analysed cells allowed us to examine how donor or acceptor concentrations influenced FRET efficiency. The N_{FRET} for individual cells expressing mG10 or mCh+eG were plotted as a function of acceptor concentration (Figure 3H). The differences in N_{FRET} were relatively constant except at the highest acceptor concentrations, where N_{FRET} from the mG10 fusion protein increased more rapidly with concentration than mCh+eG. However, the population estimates for FC-FRET represent primarily the intrinsic FRET efficiency. Moreover, the estimated N_{FRET} shows good agreement between FC-FRET and acceptor photobleaching CM-FRET efficiencies and qualitative agreement with sensitized emission CM-FRET. One possible reason for the difference in N_{FRET} measurements between FC-FRET and acceptor photobleaching CM-FRET is a potentially biased selection in the latter method of cells that have a high expression level. In addition, acceptor photobleaching CM-FRET uses a restricted subcellular region selected for measurement, with a potentially higher level of

fluorescence, while FC-FRET uses the fluorescence signal from entire cell. Nevertheless, these results show that FC-FRET is a quantitative method for determining FRET efficiency in a large number of cells rapidly with comparable sensitivity to microscopic methods.

Measurement of FRET between Crx donor and acceptor.

We used flow cytometry to examine potential FRET between individual human Crx molecules with terminal fusions with mCherry (m) or eGFP(e) (Figure 3A) expressed in HEK293T cells. Both mCrx (see Figure 3 legend for nomenclature) and Crxe were distributed exclusively in the nucleus and had a nonhomogeneous distribution (Figure 3B). N_{FRET} was highest (3.3%, $p<0.001$, one way ANOVA, Holm-Sidak, pairwise comparison with all other groups) when both donor and acceptor were fused to the N-terminus near the homeodomain (Figure 3C). N_{FRET} was lower when the fusion proteins were on the C-terminus following the activation domain and not significantly different compared to mCh+eG (1.6%, $p=0.452$, one way ANOVA, Holm-Sidak). N_{FRET} was at background levels comparable with mCh+eG when the fusion proteins were on different termini (Crxm+eCrx, $p=0.828$ and mCrx+Crxe, $p=0.917$, one way ANOVA, Holm-Sidak). Cells transfected with Crx fusion proteins together with a soluble fluorescent protein also exhibited background FRET signals (Figure 3C).

We examined the FRET signal from the various Crx fusion proteins as a function of expression level. N_{FRET} was significantly higher at all fluorescence levels when both donor and acceptor were fused to the N-terminus near the homeodomain (mCrx+eCrx) in comparison to all other combinations (Figure 3D). The slope for the mCrx+eCrx pair

increased much faster as expression levels increased compared to mCh+eG or pairs with fluorophores on opposite termini (eCrx+Crxm and Crxe+mCrx), which were similar to mCh+eG at all concentrations. N_{FRET} for constructs with fluorophores fused to the C-terminus near the activation domain (Crxe+Crxm) were intermediate between mCrx+eCrx, showing elevated N_{FRET} at higher expression levels than expected from stochastic FRET alone (57). These data indicate that a fraction of Crx molecules expressed in HEK293T cells are close enough for FRET, with fusions having both donor and acceptor near the homeodomain giving larger FRET signals than with fusions both near the activation domains. These results suggest that the FRET-detectable fraction of Crx molecules is arranged in a head to head fashion.

Measurement of FRET between Nrl donor and acceptor.

We used flow cytometry to examine potential FRET between individual human Nrl molecules with terminal fusions with mCherry or eGFP (Figure 3A) expressed in HEK293T cells. Both mNrl and Nrle were distributed exclusively in the nucleus and had a nonhomogeneous distribution (Figure 3B). N_{FRET} was highest (5.3%) and significantly different from all other groups ($p<0.001$, one way ANOVA, Holm-Sidak, pairwise comparison) when both donor and acceptor were fused to the C-terminal bZIP domain (Figure 3C). N_{FRET} was lower (2.5%) when the fluorescent proteins were both fused to the N-terminus but was significantly different than mCh+eG ($p<0.001$, one way ANOVA Holm-Sidak). N_{FRET} was at background levels for Nrlm+eNrl ($p=0.349$, one way ANOVA, Holm-Sidak, compare with mCh+eG) but slightly higher for mNrl+Nrle (2.1%, $p=0.013$, one way ANOVA, Holm-Sidak). This may reflect differences in relative angles between the

fluorophores in the two complementary pairs. Control experiments in which cells were transfected with an Nrl-fusion protein and a soluble fluorescence protein (mCherry or eGFP) exhibited N_{FRET} comparable to mCh+eG (Figure 3C).

We examined the FRET signal from the various Nrl fusion proteins as a function of expression level. Fusions to the C-terminus, near the bZip DNA binding domain, did not give expression levels as high as fusions to the N-terminus or for Crx fusion proteins (compare Figures 3D and 3F). However, N_{FRET} was much higher at all fluorescence levels when both donor and acceptor were fused to the C-terminus (Nrlm+Nrle) in comparison to all other combinations (Figure 3F). The slope for the Nrlm+Nrle pair increased faster as expression levels increased compared to mCh+eG. N_{FRET} from constructs with fluorophores fused to the N-terminus near the activation domain (mNrl+eNrl) also increased with expression level much faster than mCh+eG (Figure 3F). When fluorophores were fused to opposite termini (mNrl+Nrle, and Nrlm+eNrl), N_{FRET} behaviour diverged for reasons that are not clear. The mNrl+Nrle pair had similar N_{FRET} compared to mNrl+eNrl pair in the overlapping expression range, which was higher than mCh+eG. The other combination, Nrlm+eNrl, was similar to mCh+eG. The elevated N_{FRET} for three of the four Nrl combinations, particularly Nrlm+Nrle, were higher than expected from stochastic FRET alone (57). These data indicate that a fraction of Nrl molecules expressed in HEK293T cells are close enough for FRET, with fusions having both donor and acceptor near the DNA binding domain giving larger FRET signals than with fusions both near the activation domains. These results suggest that the FRET-detectable fraction of Nrl molecules is arranged in a head to head fashion. The FRET efficiency for

the C-terminal FRET pair is similar to that observed (~ 4%) for a heterodimer of Fos and Jun, both of which are bZIP proteins (49).

Measurement of FRET between Crx and Nrl donor-acceptor pairs.

We used flow cytometry to examine potential FRET between individual Crx and Nrl molecules with terminal fusions with mCherry or eGFP (Figure 3A) expressed in HEK293T cells. The nuclear distribution pattern for both Crx and Nrl when expressed in the same cell were similar but not identical (Figure 3B). We observed FRET between Crx and Nrl with a number of donor-acceptor fusion pairs (Figure 4A). Fusions at the N-termini of Nrl and Crx had the highest N_{FRET} compared to mCh+eG ($p=0.001$, one way ANOVA, Holm-Sidak). Fusions with fluorophores both located at the C-termini of Crx and Nrl had N_{FRET} higher than mCh+eG but it was not statistically significant ($p=0.45$, one way ANOVA, Holm-Sidak). Constructs with donor and acceptor on opposite termini were not different from mCh+eG (Figure 4A).

We examined FRET from the various combinations of fusion proteins as a function of expression level (Figure 4B). N_{FRET} from constructs with both donor and acceptor fused to the N-terminus (mNrl+eCrx) was statistically higher than mCh+eG at all fluorescence levels and than the other combinations when $F^A > 10^4$. The slope for the mNrl+eCrx pair increased faster as expression levels increased compared to mCh+eG, suggesting a possible concentration dependence on the proximity of mNrl and eCrx. The FRET signals for the other fusion constructs increased with expression level similar to mCh+eG. What is clear from the dependence on expression level is that the FRET signal from mNrl+eCrx is much higher than expected from stochastic FRET alone (57). These data indicate that

a fraction of Nrl and Crx molecules when expressed in HEK293T cells are close enough to FRET, with fusions having donor near the DNA binding domain of Crx and acceptor near the activation domain of Nrl giving large FRET signals.

We compared N_{FRET} between mCrx and eNrl using FC-FRET to those measured with CM-FRET (Figure 4C). Both acceptor photobleaching and sensitized emission approaches had significant N_{FRET} for N-terminal fused mNrl+eCrx when compared to mCh+eG (t-test, $p<0.001$, respectively). These data agree with the results from the FC-FRET experiments. The CM-FRET methods gave a higher estimated efficiency because the measurements were performed on nuclear regions with high fluorescence levels where both donor and acceptor overlap, while the FC-FRET measurements are derived from the entire nucleus, which may underestimate locally confined interactions. Taken together, these results confirm that a fraction of Crx and Nrl molecules in HEK293T nuclei are close enough for FRET.

Discussion

Flow cytometry FRET

Here, we report improvements in the use of flow cytometry to measure FRET efficiency (43-51). We showed that FC-FRET is sensitive enough to detect subtle differences in donor-acceptor linker lengths, and thus distance. In our implementation, we have a delay between exposure of cells to donor (488 nm) and acceptor (561 nm) excitation lasers, thus avoiding crosstalk between fluorescent proteins in the detection channels during their fluorescence lifetimes. Our implementation of FC-FRET employs one of the most widely used sensitized emission methods, called N_{FRET} (67), to calculate

FRET efficiency. N_{FRET} minimizes the dependence of FRET efficiency on the donor and acceptor fluorescence intensities. However, N_{FRET} deviates dramatically from expected behaviour when the stoichiometry of donor or acceptor are not matched well (42). We are able to address this issue by selecting cells with a desired acceptor/donor ratio where N_{FRET} is stable (56), here between 0.1 - 10 range.

We have standardized data acquisition and analysis. The FC-FRET results quantitatively agree with measurements made using two common microscopy-based methods and are comparable between different transfections and flow cytometry runs. FC-FRET analysis uses individual cell FRET efficiencies for statistical analysis and includes information on donor and acceptor fluorescence intensities. Thus, FC-FRET efficiencies are obtained across a wide range of expression levels. This allows the contribution of stochastic FRET to be characterized. FRET efficiency is determined from total cellular fluorescence, which potentially reduces bias in the (subjective) collection of cells with intense fluorescence. In summary, we have shown that FC-FRET is able to quantitatively study protein-protein interactions in live cells in a high-throughput manner.

Although FC-FRET has advantages, it shares several limitations with whole-cell microscopy and solution methods. FC-FRET does not provide detailed information on subcellular distribution, only measures average fluorescence intensity for each cell. If a donor and acceptor are concentrated in a particular location, the stochastic FRET efficiency could be higher than expected and thus be mistaken for protein-protein interactions. Therefore, it is imperative to design control fluorescent proteins that appropriately colocalize and produce the same expression levels as the candidate proteins for comparison. FC-FRET sensitivity is limited by the fraction of donor and

acceptor that can interact with each other. For example, if the donor and acceptor only interact in certain compartments, but are also found in other compartments, then the apparent FRET efficiency will be reduced. A strategy that combines microscopy and flow cytometry would overcome this limitation.

FRET between Nrl and Crx molecules

We obtained FRET efficiencies between Crx and Nrl that likely reflect dimer interactions of these transcription factor in *in vivo* complexes. A qualitative summary of the FRET signals and possible schematic models for the various complexes are shown (Figure 5). Our results show that a fraction of Nrl donor and acceptor fusion proteins, when expressed in the same cell, are close enough to generate a large FRET signal. The same was found with Crx donor and fusion pairs co-expressed in the same cell. These results support the conclusion that both Crx and Nrl can assemble into homodimers (or oligomers with two Crx or Nrl molecules near each other) in live cells. We found that placing donors and acceptors near the DNA binding domains (bZip for Nrl and homeodomain for Crx) gave the largest FRET signals for Nrl-Nrl or Crx-Crx pairs. These results are consistent with a parallel orientation of oligomeric Crx (head-to-head) or Nrl (tail-to-tail). In the case of Crx and Nrl, N_{FRET} was small but significantly greater than mCh+eG controls. Moreover, N_{FRET} steadily increased as expression levels increased (Figure 4B), at a rate much faster than observed for stochastic FRET. In this way, FC-FRET allows a direct examination across the entire range of fluorophore expression, permitting a qualitative separation of the FRET signal into intrinsic and stochastic components by comparison with co-expressed, unlinked donor and acceptor. This is particularly important when FRET efficiency between interacting proteins is low because

of distance, fluorophore orientation, competing cellular binding partners or influence of the K_D on extent of interaction, as examples. However, the strong FRET signals from Crx and Nrl donor-acceptor pairs, distinctly higher than control donor-acceptor pairs, demonstrate formation of Crx-Nrl complexes in live nuclei for the first time. This data is consistent with biochemical (36) and functional data (7, 36, 37) that show their interaction suggests possible mechanisms for their cooperative activity.

It is important to emphasize that we do not know what fraction of donor or acceptors expressed in the nuclei of HEK293T are available to interact or potentially participate in FRET. We are not able to determine that FRET fraction using CM-FRET approaches – additional studies require techniques such as single molecule FRET (68, 69). Because of this limitation, we are not able to estimate even relative distances between the donor and acceptors fused to Crx or Nrl. However, Nrl is part of the large Maf family and forms homo- and heterodimers with other bZip transcription factors (35). Therefore, it seems likely that Nrl will not be monomeric in HEK293T cells, rather we expect that Nrl could be in complexes with itself or other proteins as there are other Mafs and bZip proteins expressed in HEK293T cells (70). If we make the simplifying assumption that all the expressed Nrl protein was involved in FRET interactions, then using the calibration of N_{FRET} from the mG fusion series and assuming similar donor-acceptor orientations, the FC-FRET data (Figure 2E) would imply that the donor and acceptors at the C-terminal (bZip) region between Nrl monomers are ~6-7 nm apart, much closer than ~10 nm FRET detection limit. Using the total fluorescence intensity in the N_{FRET} calculation leads to an underestimation of the actual FRET efficiency and thus proximity. Nonetheless, N_{FRET} estimates seem reasonable given the following distance

estimates: 1) the structure of the closely related MafA (DNA binding domains for the MafA dimer bound to DNA are ~1 nm apart, PDB ID: 4EOT (71)), 2) the diameter of donor-acceptor molecules (~2.5 nm, (72)) and 3) the length of the $(Gly)_5$ linkers between the fluorophores and Nrl (~2 nm). This calculation further supports the identification of the N_{FRET} measure with FC-FRET as a true proximity indicator.

Conclusions

We have developed FC-FRET, an improved flow cytometry-based FRET method that validated using confocal microscopy FRET methods. The most significant advantage is the ability to analyze FRET signals from cells with a wide range of expression levels. The permits a separation of the FRET signal into intrinsic and stochastic components. Using this approach, we have observed interactions and proposed orientations between Nrl and Crx homodimers. Moreover, we have shown for the first time an interaction between Crx and Nrl in live cells.

Materials and Methods

Expression constructs

Fusion constructs and large deletions were generated by overhang extension PCR (73) using primers from IDT (IDT, Coralville, IA) and cloned Pfu DNA polymerase (Stratagene, La Jolla, CA). Point mutations and small deletions or insertions were generated using QuickChange (74) with Turbo Pfu DNA polymerase (Stratagene, La Jolla, CA). A nuclear localization signal (NLS), MAPKKKRKVNRSKA, was added at the N-termini of eGFP and mCherry (Clontech, Mountain View, CA). For intramolecular FRET experiments, eGFP

and mCherry fusion proteins (mG) were designed with various linkers (Supplemental Table 1). The α-helical linkers were based on a repeated (n=2-7) α-helix-forming peptide, EAAAK (27) flanked by two proline residues to terminate the α-helical region. For expression of Nrl and Crx fusion proteins, coding regions were cloned downstream of the CMV promoter in derivatives of the pEGFP-N1 plasmid (Clontech) with an NLS and linker sequences to eGFP or mCherry (Supplemental Table 2). All constructs were confirmed by DNA sequencing (Genewiz, www.genewiz.com).

Mammalian cell culture and transfection

HEK293T cells (ATCC, Manassas, VA) were cultured in DMEM supplemented with 10% FBS and 1 mM L-glutamine. Cells were seeded at 75,000 cells/ml one day before transfection. Cells were transfected with a total of 1 μg of DNA using Fugene 6 (Roche, Branchburg, NJ) according to the manufacturer's instructions

Confocal Microscopy FRET

In sensitized emission FRET and live cell imaging experiments, HEK293T cells were seeded on a collagen coated No. 1 coverslip placed in the bottom of a 3.5 cm dish (MatTek, Ashland, MA) before transfection. One day after transfection, cells were placed in phenol red-free DMEM (Gibco, Carlsbad, CA) containing 0.1 μg/ml Hoechst 33342 (Sigma-Aldrich, St. Louis, MO), 10% FBS and 1 mM L-glutamine and incubated for one hour. Cells were then placed in the environmental chamber (PeCon GmbH, Germany) of the confocal microscope in 5% CO_2 at 37°C and equilibrated for 15 min. Confocal images were collected using a LSM510 META microscope (Carl Zeiss, Germany) equipped with

a Plan-Apochromat 63× oil immersion objective (NA 1.4) and an Argon laser (488 nm) and a HeNe laser (543 nm). The pinhole was adjusted to obtain 1 Airy unit for the 488 nm laser. To reduce contamination signals between the two fluorescence channels, 500-535 nm band pass and 560LP long pass filters were used to filter fluorescence excited by Ar and HeNe lasers, respectively. The FRET signal was detected using the Argon laser 488 nm line and a 560LP long pass filter. Hoechst 33342 staining was detected using a two-photon Chameleon laser exciting at 800 nm (power 4-8%) and a 435/485 nm band pass filter. For dual color acquisition, 12-bit images were sequentially acquired in a line-scan mode (average of two scans). The images were filtered by one-time Gaussian blur (0.5 sigma) in ImageJ (NIH) to reduce noise. The fluorescence intensity for sensitized FRET analysis was quantified from the filtered images (N_{FRET}, details described in FC-FRET section). For presentation in the figures, filtered image brightness and contrast were adjusted using ImageJ for the entire image. In APB FRET, HEK293T cells were seeded in 8 well chamber slides (Nunc Lab-Tek), transfected as described above and then fixed with 2% paraformaldehyde for 15 min. Slides were mounted in glycerol prior to image acquisition as described above. Acceptor was sequentially photobleached using the HeNe laser at 100% power. Images were analyzed using Image J software (NIH) and Sigma Plot 11.0 (Systat Software, Inc., Chicago, IL).

Flow cytometry FRET

Cells were transfected as described above, treated with 0.1% trypsin for 5 min and then washed in phenol red-free DMEM containing 10% FBS. Cells were centrifuged at 250 g for 5 min and suspended with phosphate buffered saline at ~10^6 cells/ml. FC-FRET

measurements were performed using a LSRII flow cytometer (BD Bioscience) equipped with 405 nm, 488 nm, 561 nm and 633 nm lasers. A 19 μs delay was set between 488 nm and 561 nm laser interrogation times. To measure eGFP and FRET fluorescence intensities, cells were excited with the 488 nm laser line with fluorescence collected in the eGFP channel through a 530/30 band pass filter, while the FRET signal was collected through a 610/20 band pass filter. To measure mCherry fluorescence, cells were excited with the 561 nm laser line and fluorescence was collected through a 610/20 band pass filter. Channel settings were optimized and calibrated as follows. First, the voltage of each photomultiplier was adjusted to balance the fluorescence intensity for eGFP and mCherry. Second, the fluorescence intensity for each channel was calibrated with beads having known amounts of fluorophore attached (Spherotech, Inc.). Finally, the FSC (forward scattering) and SSC (side scattering) were calibrated with beads of known size (Spherotech, Inc). The concentration of fluorescence molecules was estimated by the fluorescence intensity and estimated size of each cells. We calibrated the fluorescence intensity and size measurement with Spherotech beads as described above. We converted intensity to equivalent brightness of fluorescence dyes (such as eGFP). We use this number to estimate the number of fluorescence molecules in a cell. We used the size standard beads to estimate the size of cells with FSC and SSC reading. We assume a HEK293 cell can approximate to a spherical ball in a solution. Based on this assumption, we estimate the volume of each cell and then the concentration of fluorescence molecules based on the number of fluorescence molecules in a cell.

For each experiment, four control groups were analysed. Mock transfected cells were used to set background fluorescence levels for donor, FRET and acceptor channels.

Cells expressing only eGFP were used to measure the bleed-through of donor emission (eGFP) into the FRET channel (610/20), calculated as the ratio of donor emission detected in the FRET (acceptor) channel to donor channel, D_C. Similarly, cells expressing only mCherry were used to measure the excitation of acceptor (mCherry) by donor excitation light (488 nm), calculated as the ratio of acceptor emission with donor excitation to acceptor fluorescence, A_C. The variation in D_C and A_C between cells decreased as both acceptor and donor fluorescence intensity increased, respectively, and we used a value of 30% variation in D_C and A_C to set the lower limit of eGFP and mCherry intensities for including cells in the analysis. We used a sensitized emission calculation, also called the three-cube method (53), to determine the normalized FRET efficiency in FC-FRET:

$$N_{FRET} = \frac{F^{DA} - Ac * F^{D} - Dc\ F^{A}}{\sqrt{F^{D} \times F^{A}}}$$

where $F^{DA}, F^{D} and\ F^{A}$ are the fluorescence intensities in the FRET, donor and acceptor channels, respectively. Flow cytometry data files were imported to custom software for data processing in the Matlab (Mathworks, Inc) environment (executable program available upon request). Different group mean or median values were compared with Student's t-test (if normality test failed, a Mann-Whitney Rank Sum test was used) or ANOVA analysis (Holm-Sidak method) in Sigma Plot 11.0 (Systat Software, Inc., Chicago, IL) using $p<0.05$(*), $p<0.01$(**) and $p<0.001$(***).

Simulation of stochastic (collisional) FRET

To simulate the effect of concentration on unlinked donor-acceptor fluorophores, we used the approach as described by Lakowicz for freely diffusing donor-acceptor pairs (57-59). To calculate the FRET efficiency for collisional events we used

535 $E = \sqrt{\pi} \times \Gamma \times exp(\Gamma^2) \times |1 - erf(\Gamma)|$, where $\Gamma = \frac{[A]}{A_0}$ is the ratio of effective acceptor
536 concentration to the critical concentration A_0, which represents the acceptor concentration
537 that results in 76% energy transfer. In the case of mCherry and eGFP, we calculated the
538 stochastic FRET to be greater than ~1% when the concentrations of mCherry and eGFP
539 are higher than ~20 μM (Figure S8A). The result of the acceptor concentration dependent
540 FRET measurement with mCherry and eGFP is close to this value (~10 μM), suggesting
541 the FRET efficiency above this level will have a stochastic FRET component. However,
542 this analysis of stochastic FRET does not include an exclusion volume for large
543 fluorophores. To include that variable in simulations of a three dimensional collisional
544 system, we used a Monte Carlo approach based on a randomized static distribution of
545 acceptors and donors (Figure S8B) to calculate the FRET efficiency by proximity using
546 the Förster equation and summing over the closest pairs. In this simulation, we used κ^2 =
547 0.476 (instead of 2/3), resulting in an energy transfer for eGFP-mCherry at the critical
548 concentration, A_0 = 3.6 mM, to be $E = 76\% \times \frac{0.476}{0.667} = 54\%$. The simulations (using in
549 MatLab (Natick, MA), R2012b) were performed over a range of concentrations (total
550 molecules 50-600) in volumes of spheres with radii of 100-600 nm and differing distance
551 constraints (3-6 nm) for the FRET efficiency calculation. A total of 21 random distributions
552 were used to generate Figure S8C.

553 **Acknowledgments**

554 This work was supported in part by the National Institutes of Health grants EY-11256 and
555 EY-12975 (B.E.K.) and the Research to Prevent Blindness (Unrestricted Grant to SUNY
556 UMU Department of Ophthalmology). We thank Dr. S. Reks critical comments on this
557 work as it progressed.

References

1. S. Blackshaw, R. E. Fraioli, T. Furukawa, C. L. Cepko, Comprehensive analysis of photoreceptor gene expression and the identification of candidate retinal disease genes. *Cell* **107**, 579-589 (2001).
2. V. Y. Arshavsky, M. E. Burns, Photoreceptor signaling: supporting vision across a wide range of light intensities. *J Biol Chem* **287**, 1620-1626 (2012).
3. R. S. Molday, O. L. Moritz, Photoreceptors at a glance. *J Cell Sci* **128**, 4039-4045 (2015).
4. J. N. Pearring, R. Y. Salinas, S. A. Baker, V. Y. Arshavsky, Protein sorting, targeting and trafficking in photoreceptor cells. *Prog Retin Eye Res* **36**, 24-51 (2013).
5. K. M. Bujakowska, Q. Liu, E. A. Pierce, Photoreceptor Cilia and Retinal Ciliopathies. *Cold Spring Harb Perspect Biol* **9,** a028274 (2017).
6. H. May-Simera, K. Nagel-Wolfrum, U. Wolfrum, Cilia - The sensory antennae in the eye. *Prog Retin Eye Res* **60**, 144-180 (2017).
7. S. Chen *et al.*, Crx, a novel Otx-like paired-homeodomain protein, binds to and transactivates photoreceptor cell-specific genes. *Neuron* **19**, 1017-1030 (1997).
8. T. Furukawa, E. M. Morrow, C. L. Cepko, Crx, a novel otx-like homeobox gene, shows photoreceptor-specific expression and regulates photoreceptor differentiation. *Cell* **91**, 531-541 (1997).
9. A. K. Hennig, G. H. Peng, S. Chen, Regulation of photoreceptor gene expression by Crx-associated transcription factor network. *Brain Res* **1192**, 114-133 (2008).
10. A. Swaroop, D. Kim, D. Forrest, Transcriptional regulation of photoreceptor development and homeostasis in the mammalian retina. *Nat Rev Neurosci* **11**, 563-576 (2010).
11. A. Swaroop *et al.*, A conserved retina-specific gene encodes a basic motif/leucine zipper domain. *Proc Natl Acad Sci U S A* **89**, 266-270 (1992).
12. T. Furukawa, E. M. Morrow, T. Li, F. C. Davis, C. L. Cepko, Retinopathy and attenuated circadian entrainment in Crx-deficient mice. *Nat Genet* **23**, 466-470 (1999).
13. A. J. Mears *et al.*, Nrl is required for rod photoreceptor development. *Nat Genet* **29**, 447-452 (2001).
14. H. Y. Chen, K. D. Kaya, L. Dong, A. Swaroop, Three-dimensional retinal organoids from mouse pluripotent stem cells mimic in vivo development with enhanced stratification and rod photoreceptor differentiation. *Mol Vis* **22**, 1077-1094 (2016).
15. J. Collin *et al.*, CRX Expression in Pluripotent Stem Cell-Derived Photoreceptors Marks a Transplantable Subpopulation of Early Cones. *Stem Cells* **37**, 609-622 (2019).
16. A. Gonzalez-Cordero *et al.*, Recapitulation of Human Retinal Development from Human Pluripotent Stem Cells Generates Transplantable Populations of Cone Photoreceptors. *Stem Cell Reports* **9**, 820-837 (2017).
17. D. A. Lamba, J. Gust, T. A. Reh, Transplantation of human embryonic stem cell-derived photoreceptors restores some visual function in Crx-deficient mice. *Cell Stem Cell* **4**, 73-79 (2009).
18. D. A. Bessant *et al.*, A mutation in NRL is associated with autosomal dominant retinitis pigmentosa. *Nat Genet* **21**, 355-356 (1999).

19. C. L. Freund *et al.*, Cone-rod dystrophy due to mutations in a novel photoreceptor-specific homeobox gene (CRX) essential for maintenance of the photoreceptor. *Cell* **91**, 543-553 (1997).
20. A. Kanda, J. S. Friedman, K. M. Nishiguchi, A. Swaroop, Retinopathy mutations in the bZIP protein NRL alter phosphorylation and transcriptional activity. *Hum Mutat* **28**, 589-598 (2007).
21. K. M. Nishiguchi *et al.*, Recessive NRL mutations in patients with clumped pigmentary retinal degeneration and relative preservation of blue cone function. *Proc Natl Acad Sci U S A* **101**, 17819-17824 (2004).
22. P. K. Swain *et al.*, Mutations in the cone-rod homeobox gene are associated with the cone-rod dystrophy photoreceptor degeneration. *Neuron* **19**, 1329-1336 (1997).
23. A. Garancher *et al.*, NRL and CRX Define Photoreceptor Identity and Reveal Subgroup-Specific Dependencies in Medulloblastoma. *Cancer Cell* **33**, 435-449 e436 (2018).
24. S. K. Verbakel *et al.*, Non-syndromic retinitis pigmentosa. *Prog Retin Eye Res* **66**, 157-186 (2018).
25. J. W. Kim *et al.*, NRL-Regulated Transcriptome Dynamics of Developing Rod Photoreceptors. *Cell Rep* **17**, 2460-2473 (2016).
26. J. C. Corbo *et al.*, CRX ChIP-seq reveals the cis-regulatory architecture of mouse photoreceptors. *Genome Res* **20**, 1512-1525 (2010).
27. H. Hao *et al.*, Transcriptional regulation of rod photoreceptor homeostasis revealed by in vivo NRL targetome analysis. *PLoS Genet* **8**, e1002649 (2012).
28. M. J. Brooks, H. K. Rajasimha, J. E. Roger, A. Swaroop, Next-generation sequencing facilitates quantitative analysis of wild-type and Nrl(-/-) retinal transcriptomes. *Mol Vis* **17**, 3034-3054 (2011).
29. M. A. Kautzmann, D. S. Kim, M. P. Felder-Schmittbuhl, A. Swaroop, Combinatorial regulation of photoreceptor differentiation factor, neural retina leucine zipper gene NRL, revealed by in vivo promoter analysis. *J Biol Chem* **286**, 28247-28255 (2011).
30. A. Mo *et al.*, Epigenomic landscapes of retinal rods and cones. *Elife* **5**, e11613 (2016).
31. G. H. Peng, S. Chen, Active opsin loci adopt intrachromosomal loops that depend on the photoreceptor transcription factor network. *Proc Natl Acad Sci U S A* **108**, 17821-17826 (2011).
32. P. A. Ruzycki, X. Zhang, S. Chen, CRX directs photoreceptor differentiation by accelerating chromatin remodeling at specific target sites. *Epigenetics Chromatin* **11**, 42 (2018).
33. J. Lee, C. A. Myers, N. Williams, M. Abdelaziz, J. C. Corbo, Quantitative fine-tuning of photoreceptor cis-regulatory elements through affinity modulation of transcription factor binding sites. *Gene Ther* **17**, 1390-1399 (2010).
34. T. K. Kerppola, T. Curran, A conserved region adjacent to the basic domain is required for recognition of an extended DNA binding site by Maf/Nrl family proteins. *Oncogene* **9**, 3149-3158 (1994).
35. T. K. Kerppola, T. Curran, Maf and Nrl can bind to AP-1 sites and form heterodimers with Fos and Jun. *Oncogene* **9**, 675-684 (1994).
36. K. P. Mitton *et al.*, The leucine zipper of NRL interacts with the CRX homeodomain. A possible mechanism of transcriptional synergy in rhodopsin regulation. *J Biol Chem* **275**, 29794-29799 (2000).

37. S. E. Reks, V. McIlvain, X. Zhuo, B. E. Knox, Cooperative activation of Xenopus rhodopsin transcription by paired-like transcription factors. *BMC Mol Biol* **15**, 4 (2014).
38. M. A. White *et al.*, A Simple Grammar Defines Activating and Repressing cis-Regulatory Elements in Photoreceptors. *Cell Rep* **17**, 1247-1254 (2016).
39. J. Piehler, New methodologies for measuring protein interactions in vivo and in vitro. *Curr Opin Struct Biol* **15**, 4-14 (2005).
40. D. W. Piston, G. J. Kremers, Fluorescent protein FRET: the good, the bad and the ugly. *Trends Biochem Sci* **32**, 407-414 (2007).
41. R. N. Day, M. W. Davidson, Fluorescent proteins for FRET microscopy: monitoring protein interactions in living cells. *Bioessays* **34**, 341-350 (2012).
42. A. Zeug, A. Woehler, E. Neher, E. G. Ponimaskin, Quantitative intensity-based FRET approaches--a comparative snapshot. *Biophys J* **103**, 1821-1827 (2012).
43. C. Banning *et al.*, A flow cytometry-based FRET assay to identify and analyse protein-protein interactions in living cells. *PLoS One* **5**, e9344 (2010).
44. F. K. Chan *et al.*, Fluorescence resonance energy transfer analysis of cell surface receptor interactions and signaling using spectral variants of the green fluorescent protein. *Cytometry* **44**, 361-368 (2001).
45. L. He *et al.*, Flow cytometric measurement of fluorescence (Forster) resonance energy transfer from cyan fluorescent protein to yellow fluorescent protein using single-laser excitation at 458 nm. *Cytometry A* **53**, 39-54 (2003).
46. L. He *et al.*, A flow cytometric method to detect protein-protein interaction in living cells by directly visualizing donor fluorophore quenching during CFP-->YFP fluorescence resonance energy transfer (FRET). *Cytometry A* **55**, 71-85 (2003).
47. L. He, A. C. Grammer, X. Wu, P. E. Lipsky, TRAF3 forms heterotrimers with TRAF2 and modulates its ability to mediate NF-{kappa}B activation. *J Biol Chem* **279**, 55855-55865 (2004).
48. L. Tron *et al.*, Flow cytometric measurement of fluorescence resonance energy transfer on cell surfaces. Quantitative evaluation of the transfer efficiency on a cell-by-cell basis. *Biophys J* **45**, 939-946 (1984).
49. G. Vamosi *et al.*, Conformation of the c-Fos/c-Jun complex in vivo: a combined FRET, FCCS, and MD-modeling study. *Biophys J* **94**, 2859-2868 (2008).
50. X. You *et al.*, Intracellular protein interaction mapping with FRET hybrids. *Proc Natl Acad Sci U S A* **103**, 18458-18463 (2006).
51. X. Wu *et al.*, Prestin-prestin and prestin-GLUT5 interactions in HEK293T cells. *Dev Neurobiol* **67**, 483-497 (2007).
52. B. Camuzeaux, C. Spriet, L. Heliot, J. Coll, M. Duterque-Coquillaud, Imaging Erg and Jun transcription factor interaction in living cells using fluorescence resonance energy transfer analyses. *Biochem Biophys Res Commun* **332**, 1107-1114 (2005).
53. D. C. Youvan *et al.*, Calibration of fluorescence resonance energy transfer in microscopy using genetically engineered GFP derivatives on nickel chelating beads. *Biotechnology et alia.*, 1-18 (1997).
54. S. Marqusee, R. L. Baldwin, Helix stabilization by Glu-...Lys+ salt bridges in short peptides of de novo design. *Proc Natl Acad Sci U S A* **84**, 8898-8902 (1987).
55. A. Kitamura, Y. Nakayama, M. Kinjo, Efficient and dynamic nuclear localization of green fluorescent protein via RNA binding. *Biochem Biophys Res Commun* **463**, 401-406 (2015).

56. C. Berney, G. Danuser, FRET or no FRET: a quantitative comparison. *Biophys J* **84**, 3992-4010 (2003).
57. J. R. Lakowicz, *Principles of Fluorescence Spectroscopy* (Springer, Boston, MA, ed. 3rd, 2006), pp. 954.
58. M. G. Erickson, D. L. Moon, D. T. Yue, DsRed as a potential FRET partner with CFP and GFP. *Biophys J* **85**, 599-611 (2003).
59. E. S. Butz *et al.*, Quantifying macromolecular interactions in living cells using FRET two-hybrid assays. *Nat Protoc* **11**, 2470-2498 (2016).
60. R. Arai, H. Ueda, A. Kitayama, N. Kamiya, T. Nagamune, Design of the linkers which effectively separate domains of a bifunctional fusion protein. *Protein Eng* **14**, 529-532 (2001).
61. R. Arai, W. Wriggers, Y. Nishikawa, T. Nagamune, T. Fujisawa, Conformations of variably linked chimeric proteins evaluated by synchrotron X-ray small-angle scattering. *Proteins* **57**, 829-838 (2004).
62. W. Wriggers, S. Chakravarty, P. A. Jennings, Control of protein functional dynamics by peptide linkers. *Biopolymers* **80**, 736-746 (2005).
63. M. Tramier, M. Zahid, J. C. Mevel, M. J. Masse, M. Coppey-Moisan, Sensitivity of CFP/YFP and GFP/mCherry pairs to donor photobleaching on FRET determination by fluorescence lifetime imaging microscopy in living cells. *Microsc Res Tech* **69**, 933-939 (2006).
64. L. Albertazzi, D. Arosio, L. Marchetti, F. Ricci, F. Beltram, Quantitative FRET analysis with the EGFP-mCherry fluorescent protein pair. *Photochem Photobiol* **85**, 287-297 (2009).
65. N. Akrap, T. Seidel, B. G. Barisas, Forster distances for fluorescence resonant energy transfer between mCherry and other visible fluorescent proteins. *Anal Biochem* **402**, 105-106 (2010).
66. H. Amiri, G. Schultz, M. Schaefer, FRET-based analysis of TRPC subunit stoichiometry. *Cell Calcium* **33**, 463-470 (2003).
67. Z. Xia, Y. Liu, Reliable and global measurement of fluorescence resonance energy transfer using fluorescence microscopes. *Biophys J* **81**, 2395-2402 (2001).
68. R. Roy, S. Hohng, T. Ha, A practical guide to single-molecule FRET. *Nat Methods* **5**, 507-516 (2008).
69. E. Lerner *et al.*, FRET-based dynamic structural biology: Challenges, perspectives and an appeal for open-science practices. *Elife* **10** (2021).
70. M. Malm *et al.*, Evolution from adherent to suspension: systems biology of HEK293 cell line development. *Sci Rep* **10**, 18996 (2020).
71. X. Lu, G. P. Guanga, C. Wan, R. B. Rose, A novel DNA binding mechanism for maf basic region-leucine zipper factors inferred from a MafA-DNA complex structure and binding specificities. *Biochemistry* **51**, 9706-9717 (2012).
72. M. Ormo *et al.*, Crystal structure of the Aequorea victoria green fluorescent protein. *Science* **273**, 1392-1395 (1996).
73. R. Higuchi, B. Krummel, R. K. Saiki, A general method of in vitro preparation and specific mutagenesis of DNA fragments: study of protein and DNA interactions. *Nucleic Acids Res* **16**, 7351-7367 (1988).
74. J. Braman, C. Papworth, A. Greener, Site-directed mutagenesis using double-stranded plasmid DNA templates. *Methods Mol Biol* **57**, 31-44 (1996).

FIGURES

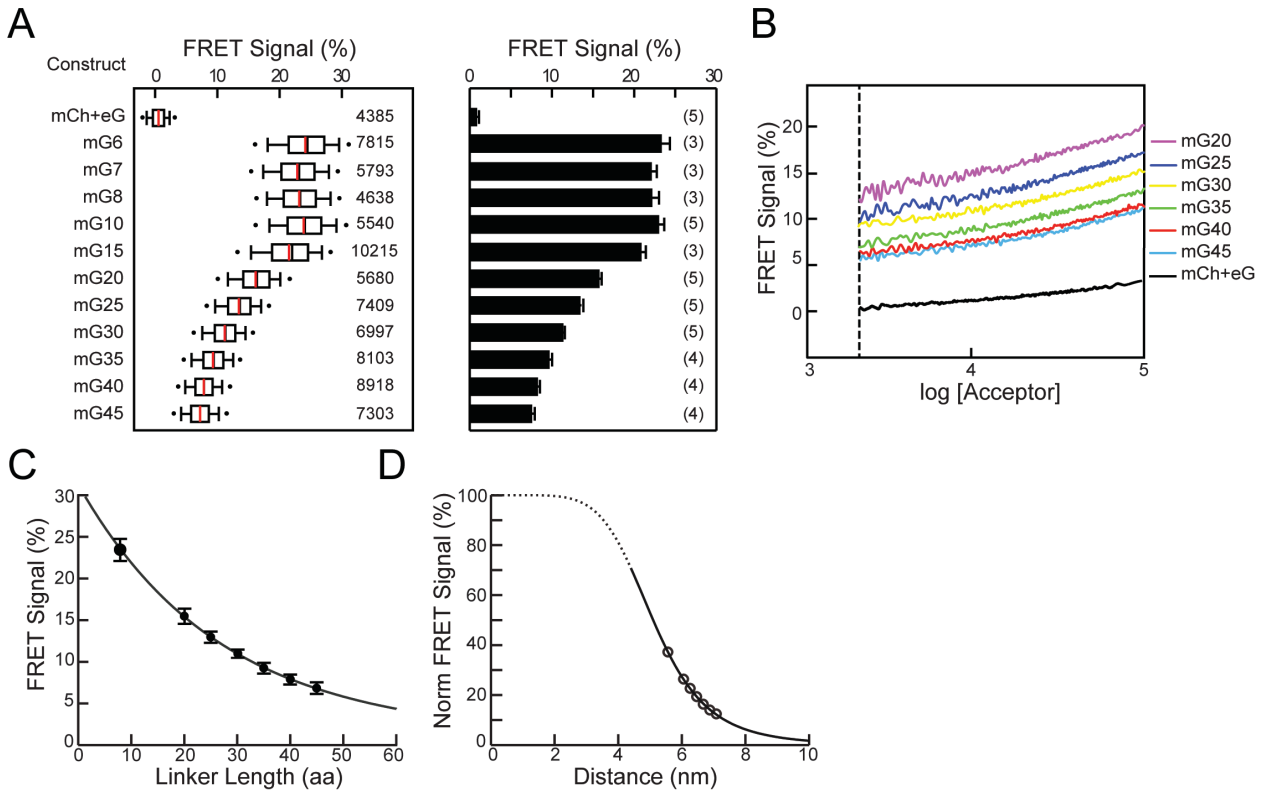

Figure 1. Flow cytometry FRET.

A) Comparison of FRET signals (N_{FRET}) between mCherry and eGFP fusion constructs (mGx) that contain linkers of different length (x = number of amino acids) in a single flow cytometry run (*left panel*) or averaged over multiple experiments (*right panel*). For the single experiment, results are shown as box plot, with mean (*red lines*) and median (*black lines*) values indicated, with the number of cells analysed to the right of the box. For averaged experiments, mean values with SEM of the FRET signals are shown in a bar graph, with the number of experiments in parentheses. B) The FRET signals from cells expressing mG20-45 from a single flow cytometry run. The distribution range of cell acceptor fluorescence intensities was divided into intervals with 100 cells in each bin. In the intensity plot, a moving average of N_{FRET} was calculated and are plotted versus the acceptor intensity in that bin. Error bars are suppressed for clarity. C) Mean N_{FRET} with SEM from the averaged experiments (A) are plotted as a function of linker length for mG8 and mG20-45. The line is a fit (R^2= 0.998) to the Förster equation modified to use linker length with the parameters k_1=0.27, k_2=5.56. (D) Normalized FRET signals from C plotted as a function of predicted distance fit to the FRET equation (*solid black line*) with the same parameters in C. Dashed line indicates the inaccessible distance between mCherry and eGFP due to steric volume exclusion between the two fluorescent proteins.

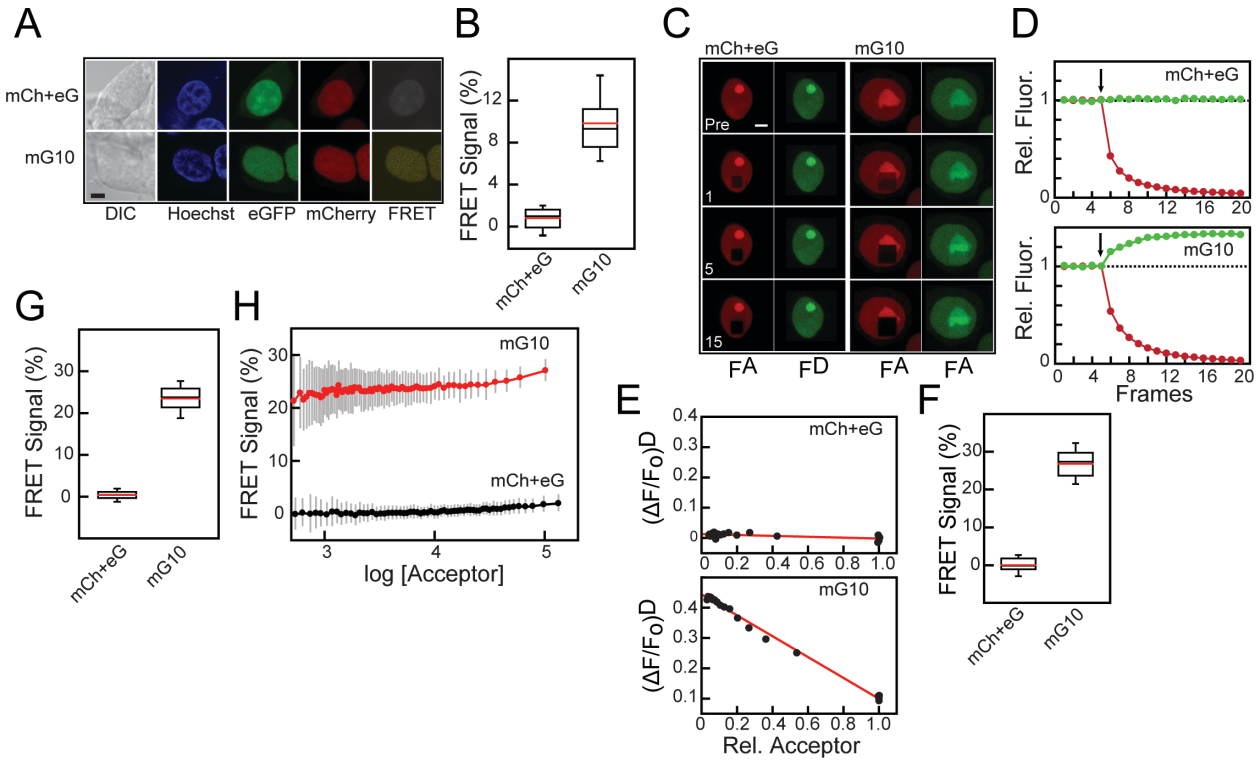

Figure 2. Comparison of confocal microscopy and flow cytometry FRET.

A) Confocal microscopy images show HEK293 cells expressing both mCh and eG (mCh+eG, *top panels*) or an mCherry-eGFP fusion protein with a 10 amino acid linker (mG10, *bottom panels*). DIC, Hoechst (*blue*), eGFP (*green*), mCherry (*red*), FRET (*yellow*). Scale bar is 5 μm. B) Box plot showing the mean (*red line*) and median (*black line*) for sensitized emission N_{FRET} for mG10 (n=37) and mCh+eG (n=31). C) Sequential confocal microscopy images of cells expressing mCh+eG (*left panels*) and mG10 (*right panels*) before and after photobleaching. Regions were bleached after each frame with a 543 nm laser and imaged in both mCherry and eGFP channels before bleaching (*Pre*) and after 1, 5 and 15 laser pulses as. D) Fluorescence intensity changes during acceptor photobleaching in cells from (C) expressing mCh+eG (*top panel*) or mG10 (*bottom panel*). mCherry intensity (*red*) and eGFP intensity (*green*) are shown. Arrow indicates start of photobleaching. E) Plots summarizing fluorescence changes after sequential bleaching with 543 nm laser. The ordinate is the remaining acceptor fluorescence while the abscissa the fraction of donor fluorescence remaining. Measurements of relative fluorescence intensity after each bleaching laser pulse are shown (*black circles*) and the lines are a linear fit. F) Box plots showing the mean (*red lines*) and median (*black lines*) N_{FRET} from accepter photobleaching experiments for mG10 (n=37) and mCh+eG (n=31). G) FRET signals obtained in a flow cytometry experiment for individual cells expressing mG10 (*red*) or mCh+eG (*black*). A moving average of N_{FRET} was calculated for bins of 100-cells and are plotted versus the acceptor intensity in that bin. Error bars (*grey*) are standard deviations. H) Box plots showing the mean (*red lines*) and median (*black lines*) N_{FRET} from flow cytometry experiments for cells expressing mCh+eG (n=5267) or mG10 (n=6987).

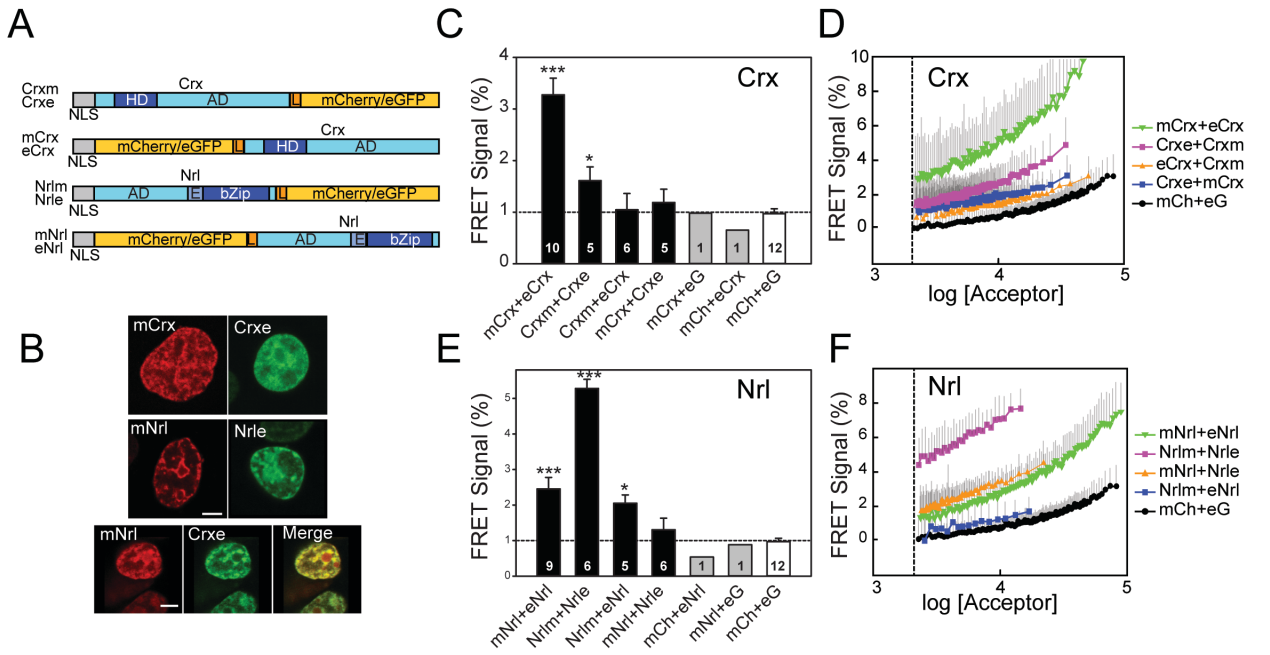

Figure 3. FRET between fluorescently tagged Crx and Nrl homo-pairs.

A) Fluorescent Crx and Nrl constructs used for FRET analysis. Diagram illustrates the fusions between fluorophores (mCherry and eGFP) and at the N and C-termini of Crx or Nrl. All constructs have an N-terminal nuclear location signal (NLS). Domains of Crx and Nrl are indicated: activation domains (AD), homeodomain (HD), basic leucine zipper domain (bZip), and linkers (L). The constructs are labeled with the fluorophore (m: mCherry or e: eGFP) at the beginning or end of the label depending upon the terminus to which it is fused. For example, mNrl is Nrl with mCherry fused to the N-terminus. B) Confocal microscopy images of transiently transfected HEK293T cells expressing fluorescently tagged Nrl labeled (*top row*), Crx (*middle row*) and both Crx and Nrl (*bottom panel*, which also contains a merged image). All constructs exhibit almost exclusively nuclear staining, with a patchy intranuclear pattern. Scale bars are 5 μm. C, E) Comparison of FRET signals determined by flow cytometry using HEK293T cells cotransfected with combinations of donor-acceptor Crx (C) or Nrl (E) fusion constructs as indicated in the panel. The bars represent mean values with standard errors of the FRET signals from the indicated number of flow cytometry experiments. For each experiment, more than 1000 cells were analyzed. Statistical significance was performed using ANOVA (compared with mCh+eG cells): $p<0.05$ (*) and $p<0.001$ (***). The samples with only a single flow cytometry experiment were not used in the ANOVA. The dotted line indicated the mean FRET signal for mCh+eG. D,F) FRET signals in individual cells expressing combinations of donor and acceptor fused to Crx (D) or Nrl (F) are plotted as a function of acceptor fluorescence intensity. Symbols are the mean FRET signal in each bin (100 cells) and lines are moving averages. Error bars (*grey*) are the SD, only the positive SD is plotted for clarity. Cells with fluorescence values below threshold fluorescence intensity (*dashed line*) were not included in the analysis.

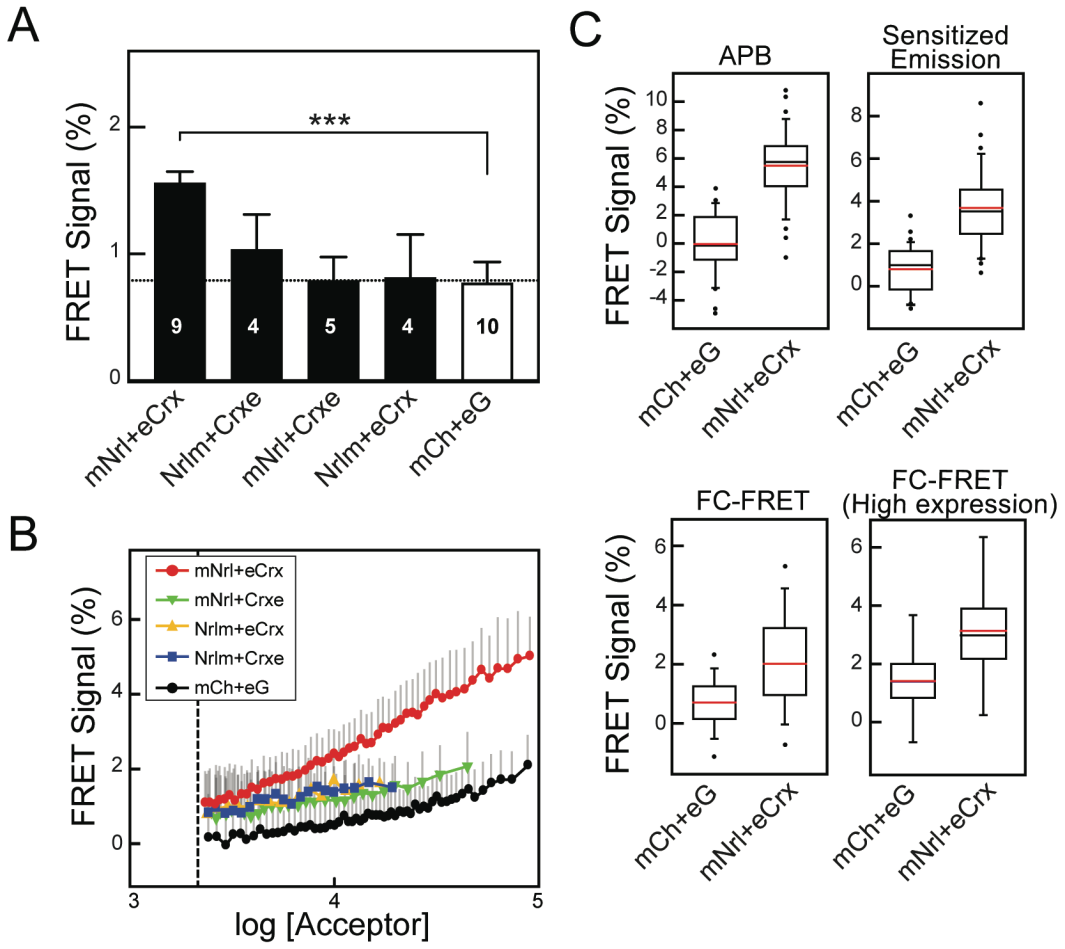

Figure 4. FRET between fluorescently tagged Crx and Nrl hetero-pairs.

A) Comparisons of FRET signals determined by flow cytometry using HEK293T cells cotransfected with combinations of donor-acceptor Crx and Nrl fusion constructs as indicated. The bars represent mean N_{FRET} with standard errors from the indicated number of flow cytometry experiments indicated. For each experiment, more than 1000 cells were analyzed. The dotted line indicates the mean FRET signal for mCh+eG. Statistical significance was determined by ANOVA and pairwise comparisons with mCh+eG cells: $p<0.001$ (***). B) FRET signals in individual cells expressing combinations of donor and acceptor fused to Crx and Nrl as indicated are plotted as a function of acceptor fluorescence intensity. Symbols are the mean FRET signal in each bin (100 cells) and lines are moving averages. Error bars (*grey*) are the SD, only the positive SD is plotted for clarity. Cells with fluorescence values below threshold fluorescence intensity (*dashed line*) were not included in the analysis. C) Box plot comparisons of FRET signals for Crx-Nrl donor and acceptors measured by microscopy-based FRET (*APB* and *Sensitized Emission*) and one flow cytometry FRET experiment. The numbers of cells analyzed (mCh+eG/mNrl+eCrx): APB, n = 31/34; Sensitized Emission, n = 31/34; FC-FRET, n = 6996/8237; FC-FRET (High-expression, $F^A > 10^4$), n = 1031/953. Mean (*red lines*) and median (*black lines*) N_{FRET} are indicated. Statistical significance for each comparison was significant by t-test with $P<0.001$ (***).

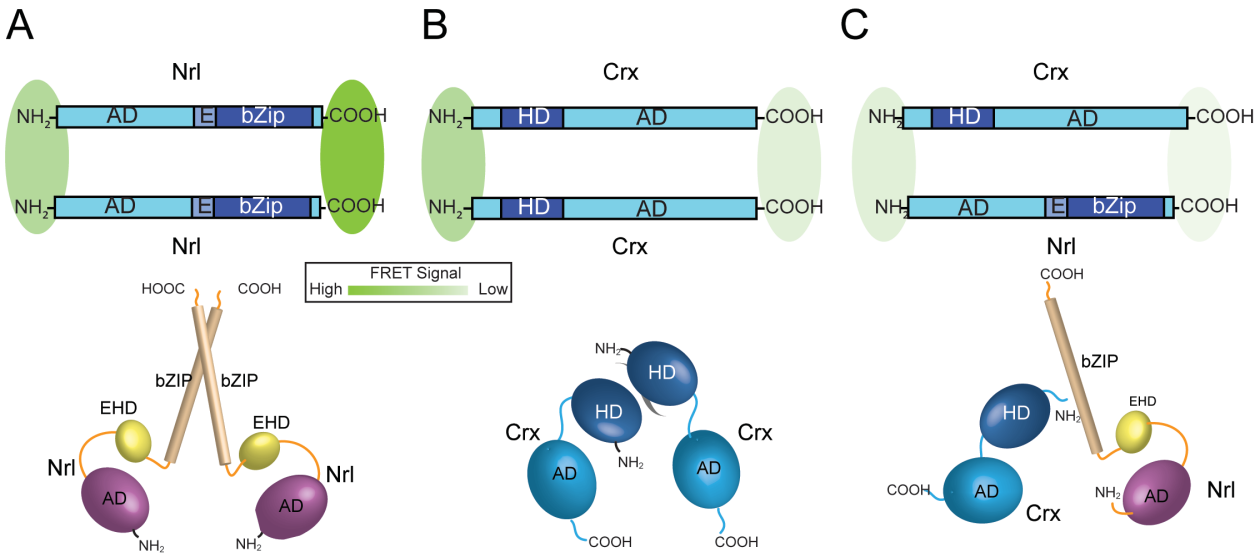

Figure 5. Models of Nrl and Crx interactions based on FRET signals.

Upper Diagrams. Schematic diagrams illustrating possible arrangements of Nrl (A) and Crx (B) homodimers and Nrl-Crx heterodimer (C). The intensity of the FRET signals obtained for the various combinations (Figures 4 and 5) are illustrated as green shaded ovals, with the intensity of the color representing the relative FRET signals for the various constructs. *Lower Diagrams*: Speculative three-dimensional arrangement of the various domains in Nrl and Crx complexes.

Supplementary Materials

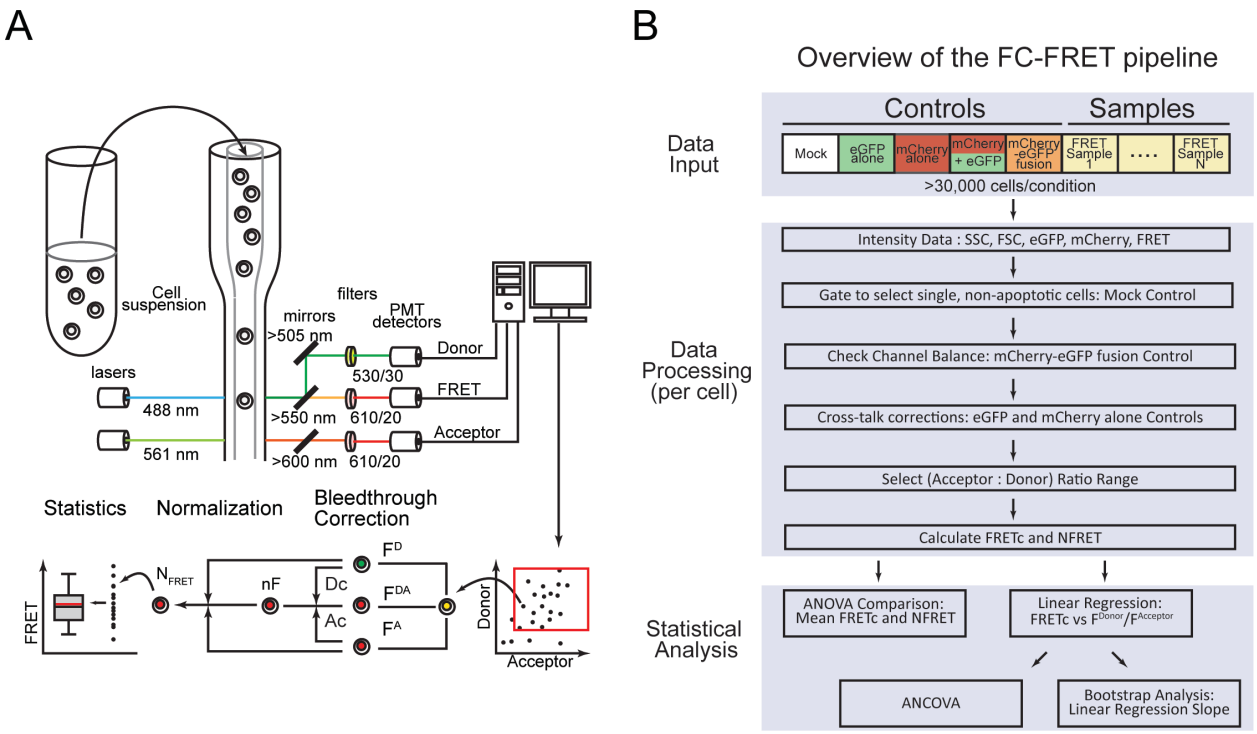

Figure S1. Flow cytometry to detect FRET signals.

The experiment setup (A) and data processing workflow (B) of flow cytometry-based FRET. Live HEK293T cells were transfected with nuclear localized mCherry-eGFP fusion proteins (mG) or transcription factors tagged with either mCherry or eGFP. Cells were analysed on a BD LSRII flow cytometer. Cell were transported in a sheath fluid and streamed to the laser beams for interrogation. Two lasers, 488 nm and 561 nm were used in this system with different focusing position. The 488nm laser excited eGFP and FRET signals, which were directed through 530/30 and 610/20 optical filters to the donor (F^{D}) and FRET PMT Channels (F^{DA}) accordingly. The 561 nm laser excited the mCherry signal that was directed through 610/20 optical filters to the acceptor PMT Channel (F^{A}). The FRET signal (F^{DA}) was corrected for background fluorescence, spill-over from donor (Dc) and excitation of acceptor (Ac). The corrected FRET signal was normalized with donor and acceptor signal to generate the FRET signal (N_{FRET}). The cell by cell FRET result then underwent further desired statistical analysis.

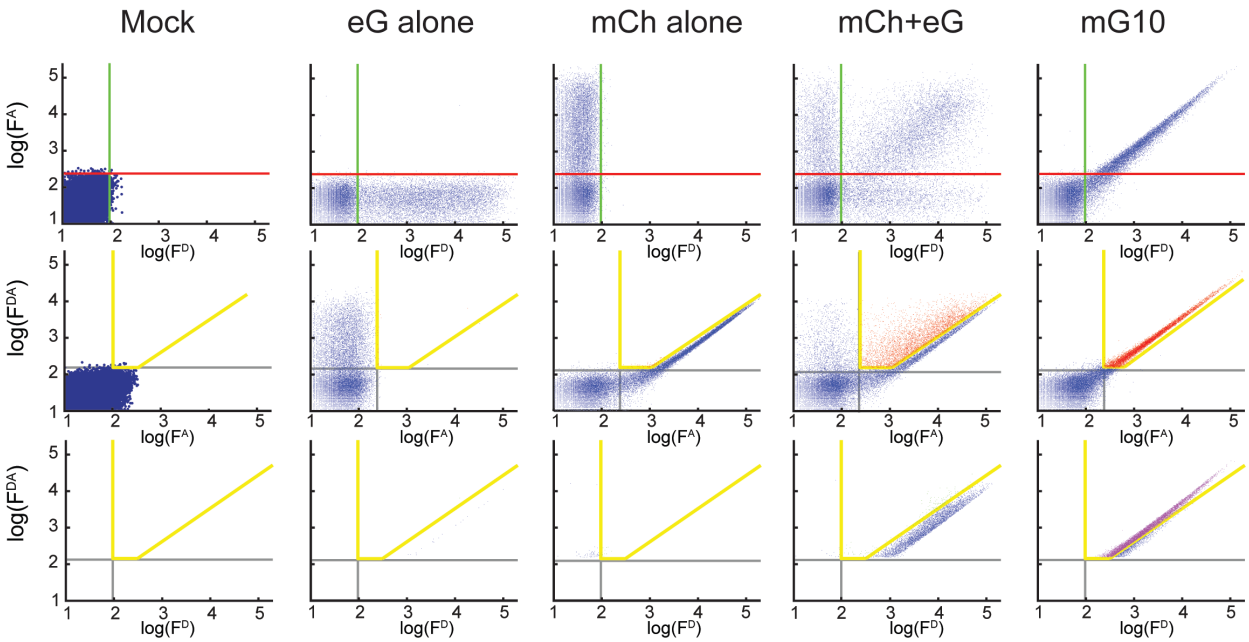

Figure S2. Fluorescence intensity distributions in HEK293T cells transfected with fluorophores analysed by multichannel flow cytometry.

Distributions of the five cell populations used in FC-FRET analysis: eGFP (F^D), mCherry (F^A) and FRET (F^{DA}) fluorescence intensities. The threshold levels for eGFP (*green*) and mCherry (*red*) fluorescence channels are shown in the top row. The FRET threshold levels after correcting for background, spill over and crosstalk are shown (yellow). Cells that cross over the FRET threshold are shown in red. Although the cell number is readily determined for the various samples, it is not possible to determine a FRET efficiency with cell counts alone. This limits the sensitivity of flow cytometry methods based on this strategy.

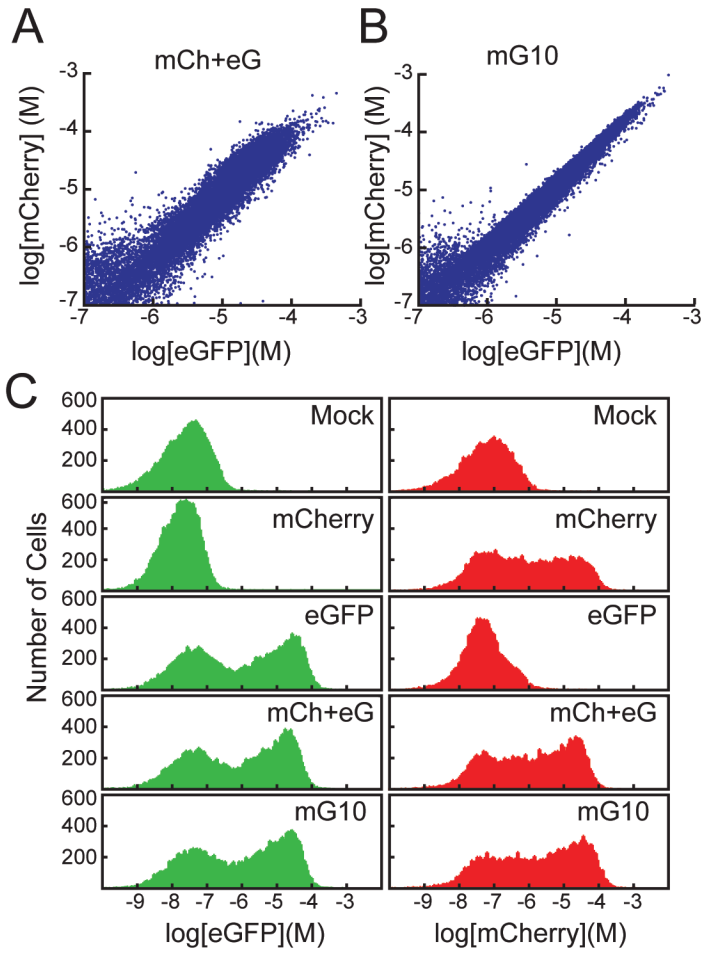

Figure S3. Expression levels and fluorescence intensities in transfected HEK293T cells.

A, B) Scatter plots of mCherry (*red*) and eGFP (*green*) concentration in HEK293T cells transfected with mCh+eG (A) and mG10 (B). Concentrations were determined from the flow data as described in Methods. C) Histograms of mCherry and eGFP expression levels in cells mock transfected or expressing mCherry, eGFP, mCherry and eGFP or an mCherry-eGFP fusion protein separated by 10 amino acids.

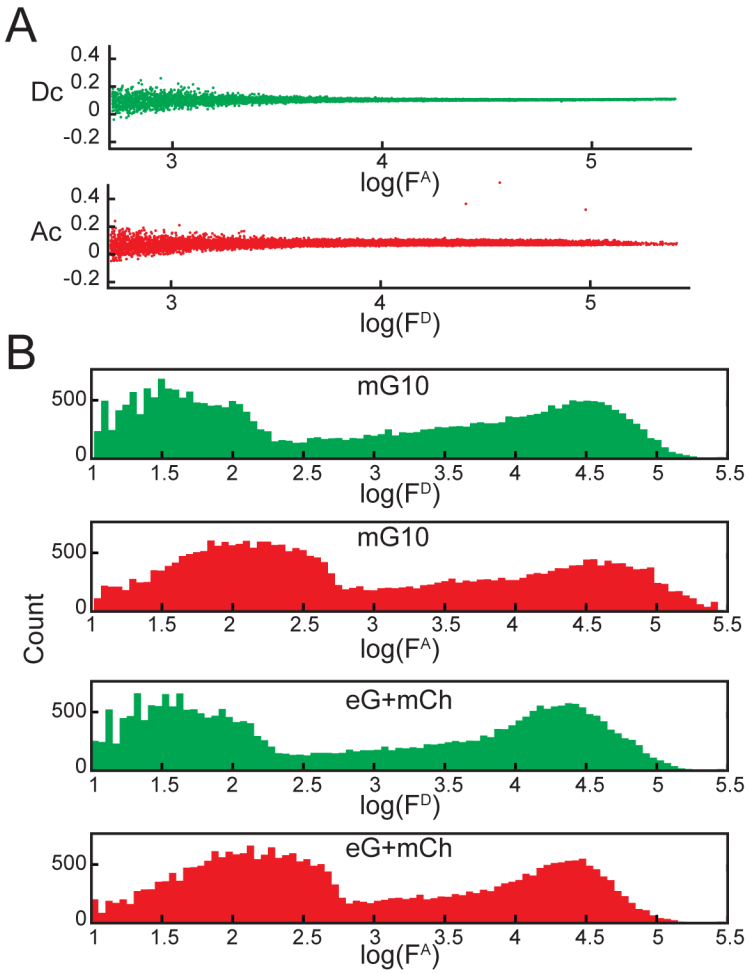

Figure S4. Comparison of the crosstalk corrections and fluorescence distributions in cells expressing fluorescent proteins analyzed by multichannel flow cytometry.

A) Scatterplots of of the donor (Dc, *top panel*) and acceptor (Ac, *bottom panel*) crosstalk corrections used to adjust the fluorescence levels prior to calculation of FRET signal. The top panel uses fluorescence from cells expressing eGFP only while the lower panel is from cells expressing mCherry only. B) Histograms of mCherry and eGFP fluorescence levels in cells transfected with mG10 fusion protein (*upper pair*) or mCherry and eGFP (*lower pair*).

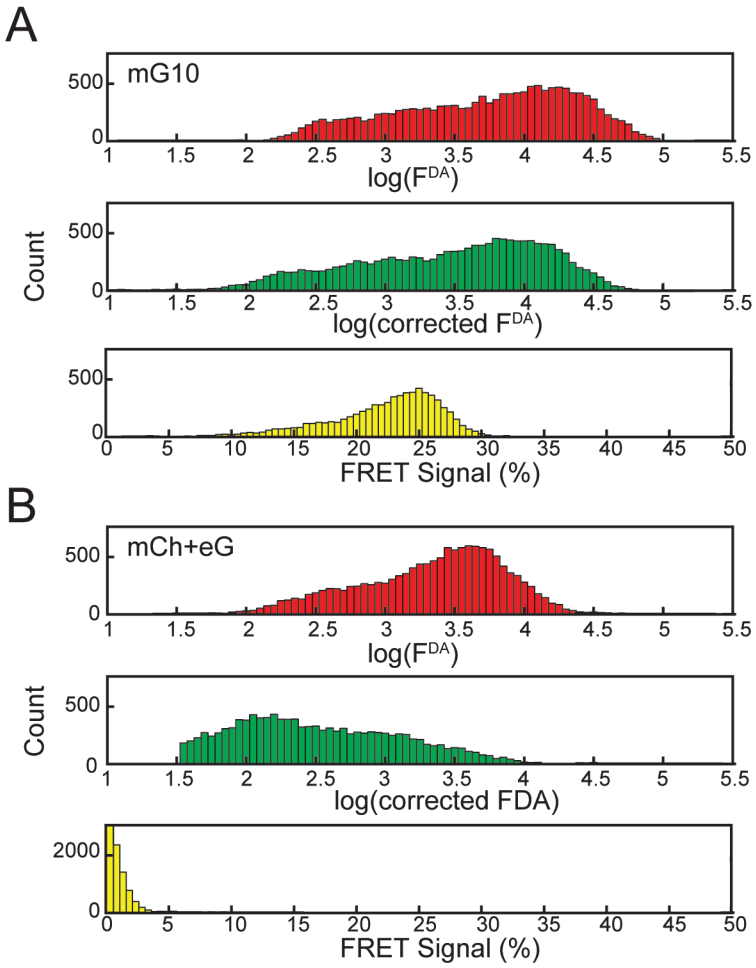

Figure S5. Calculation of N_{FRET} from flow cytometry intensities.

Histograms of fluorescence intensities from HEK293T cells expressing mG10 (A) or mCherry and eGFP (B) in the FRET channel (F^{DA}, upper panels), corrected for crosstalk (corrected F^{DA}, *middle panels*) and converted to N_{FRET} by normalization with donor and acceptor fluorescence (FRET Signal (%), *lower panels*).

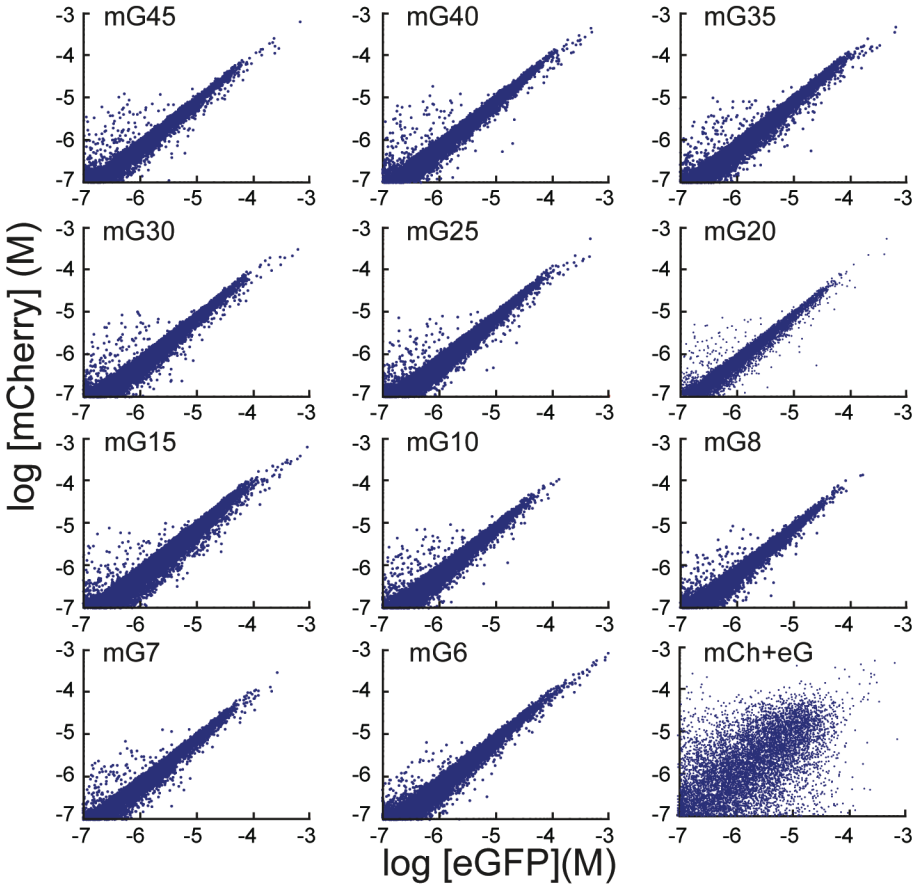

Figure S6. Multichannel flow cytometry of HEK293T cells expressing mCherry-eGFP fusion proteins separated by linkers of different lengths.

Histograms of multichannel fluorescence intensities converted to concentration from HEK293T cells expressing mG proteins.

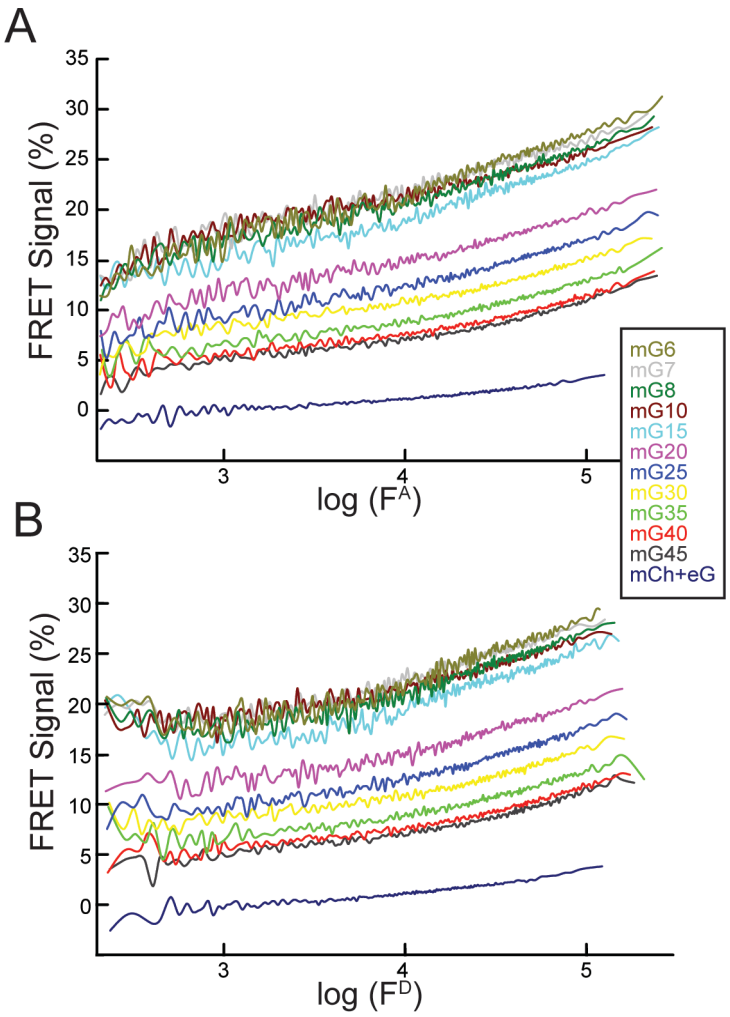

Figure S7. FC-FRET signal dependence on donor and acceptor fluorescence intensities.

FRET signals from HEK293T cells expressing mG fusion proteins are plotted as a function of acceptor (A) and donor (B) fluorescence intensity. Intensity range was divided into bins of 100 cells and the mean N_{FRET} is plotted as a moving average.

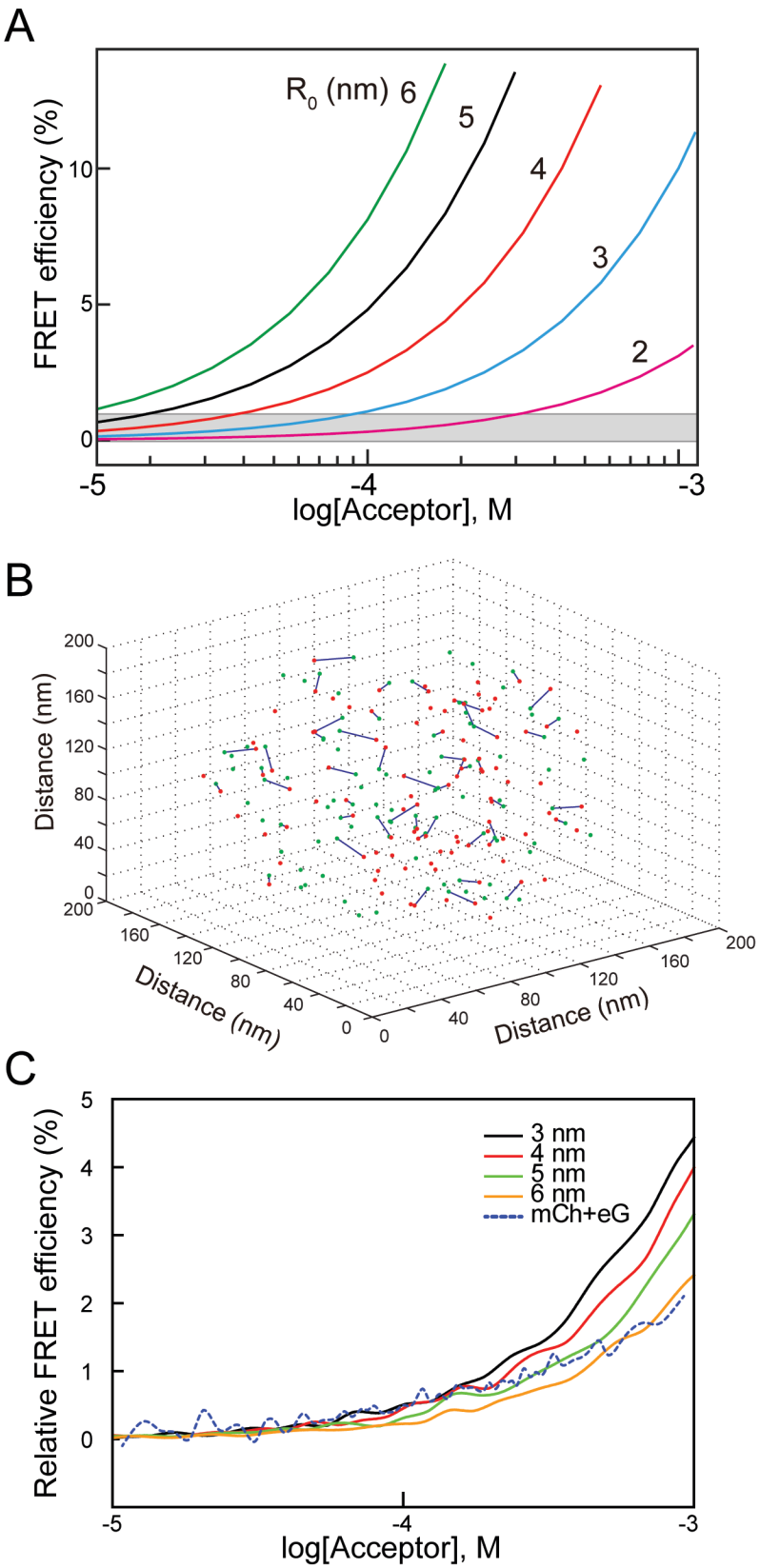

Figure S8. Stochastic FRET between mCherry and eGFP.

A. Calculation of the FRET efficiency as a function of acceptor concentration (assuming a 1:1 donor-acceptor ratio) arising from molecular collisions of freely diffusing eGFP and mCherry using the Lakowicz equation (*see* Methods). The various values of R_0 are indicated. B. Simulation including protein exclusion size. An example distribution of donor and acceptor molecules (100) randomly arranged in a sphere with a diameter of 100 nm. The distribution was generated including an exclusion zone for each fluorophore to simulate the volume of the protein core. Those pairs that met the distance criterion between the two fluorophores are connected (*lines*). C) For Monte Carlo simulation of stochastic FRET, random distributions as in (B) with different concentrations of donor-acceptor pairs were generated, the ensemble FRET efficiency calculated and then averaged to generate the relative FRET efficiency. The actual measured N_{FRET} from an FC-FRET experiment is shown (*dotted line*).

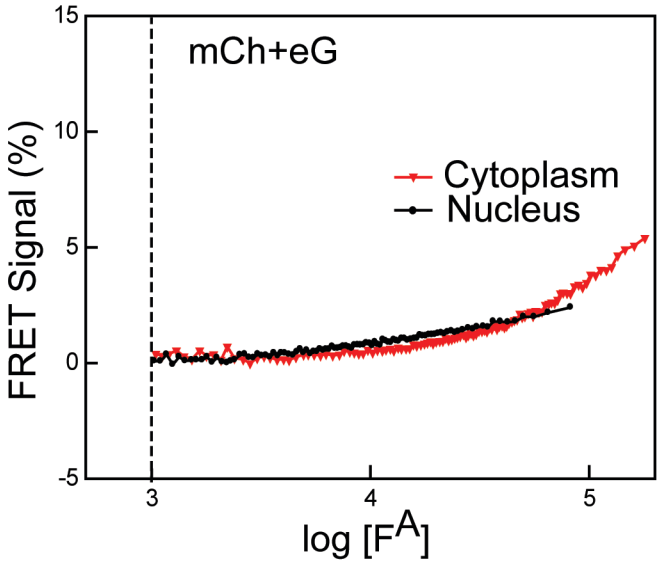

Figure S9. Comparison of FC-FRET signals from mCherry and eGFP co-expressed in HEK293T cells.

HEK293T cells were co-transfected with GFP and mCherry with (*black*) and without the nuclear localization signal (red). N_{FRET} was determined for each cell, the cells were sorted by acceptor intensity and divided into bins of 100 cells. The symbols are the mean for each bin and the line a moving average.

Supplemental Table 1
Linkers for the mCherry-eGFP fusion proteins

Name	Length aa	Amino Acid Sequence
mG6	6	NH_2-DPPVAT
mG7	7	NH_2-DPVPVAT
mG8	8	NH_2-DPAVPVAT
mG10	10	NH_2-GGGLDPPVAT
mG15	15	NH_2-GGGLDPPVATGGGGG
mG20	20	NH_2-DPGA$(EAAAK)_2$AVPVAT
mG25	25	NH_2-DPGA$(EAAAK)_3$AVPVAT
mG30	30	NH_2-DPGA$(EAAAK)_4$AVPVAT
mG35	35	NH_2-DPGA$(EAAAK)_5$AVPVAT
mG40	40	NH_2-DPGA$(EAAAK)_6$AVPVAT
mG45	45	NH_2-DPGA$(EAAAK)_7$AVPVAT

Supplemental Table 2
Linker sequences for the Crx and Nrl mCherry/eGFP fusion proteins

Construct	Amino Acid Sequence
eNrl	NH_2-MAPKKKRKVNRSKAEQKLISEEDLNSRPLE-**eGFP**-GGGGGNSSR(L)-**Nrl**
eCrx	NH_2-MAPKKKRKVNRSKAEQKLISEEDLNSRPLE-**eGFP**-GRWRWRPR-Crx
Nrle	NH_2-MAPKKKRKVNRSKAEQKLISEEDLNSS(R)-**Nrl**-GGGGG-**eGFP**
Crxe	NH_2-MAPKKKRKVNRSKAEQKLISEEDLNSSRPLE-**Crx**-GGGGG-**eGFP**
mNrl	NH_2-MAPKKKRKVNRSKAEQKLISEEDLNSGGGG-**mCherry**-GGGGGNSS(R)-**Nrl**
mCrx	NH_2-MAPKKKRKVNRSKAEQKLISEEDLNSRPLEG-**mCherry**-GGGGGGLE-**Crx**
Nrlm	NH_2-MAPKKKRKVNRSKAEQKLISEEDLNSS(R)-**Nrl**-GGGGG-**mCherry**
Crxm	NH_2-MAPKKKRKVNRSKAEQKLISEEDLNSRPLE-**Crx**-GTAGPGSGGGGG-**mCherry**

The nuclear localization sequence is underlined. The NCBI accession numbers are for human Crx, NP_000545 and human Nrl, NP_001341697. For Nrl constructs, the initiator codon was replaced by the amino acid in parentheses. eGFP and mCherry cDNAs were from Clontech.